MAMMA - vhub app

Alvaro Aravena, Mattia de'Michieli Vitturi

March 9, 2018

MAMMA is a FORTRAN90 code designed to solve a conservative model for steady magma ascent in a volcanic conduit, described as a compressible multicomponent two-phase flow. It is an open-source code (https://github.com/demichie/MAMMA) and a simplified, user-friendly version is available in vhub (https://vhub.org/tools/mamma/). In this document, we describe the part of the model related to the user-friendly version of MAMMA.

1 System of equations

The system of conservation equations is derived from the theory of thermodynamically compatible systems [1], considering the effects of the main processes that magmas experience during ascent, such as crystallization, rheological changes, fragmentation, physical interaction with conduit walls, vertical outgassing and lateral degassing. The system is described as a mixture of two phases ($i = 1, 2$), each one characterized by a volume fraction (α_i), density (ρ_i), velocity (u_i) and specific entropy (s_i). Below the fragmentation level, phase 1 is a mixture of crystals, dissolved volatiles and melt (continuous phase); while phase 2 is composed by the exsolved gas bubbles (dispersed phase). Above magma fragmentation, phase 1 is constituted by magma fragments (dispersed phase) and phase 2 is the exsolved gas mixture (continuous phase). Magma fragmentation occurs when the exsolved gas volume fraction reaches a critical value ($\alpha_g = \alpha_2 = \alpha_{cr}$) [2] (Fig. 1).

The components of the system are characterized by an equation of state; while pressure (p_i) and temperature (T_i) of both phases are derived from the internal energy (e_i):

$$p_i = \rho_i^2 \frac{\partial e_i}{\partial \rho_i} \tag{1}$$

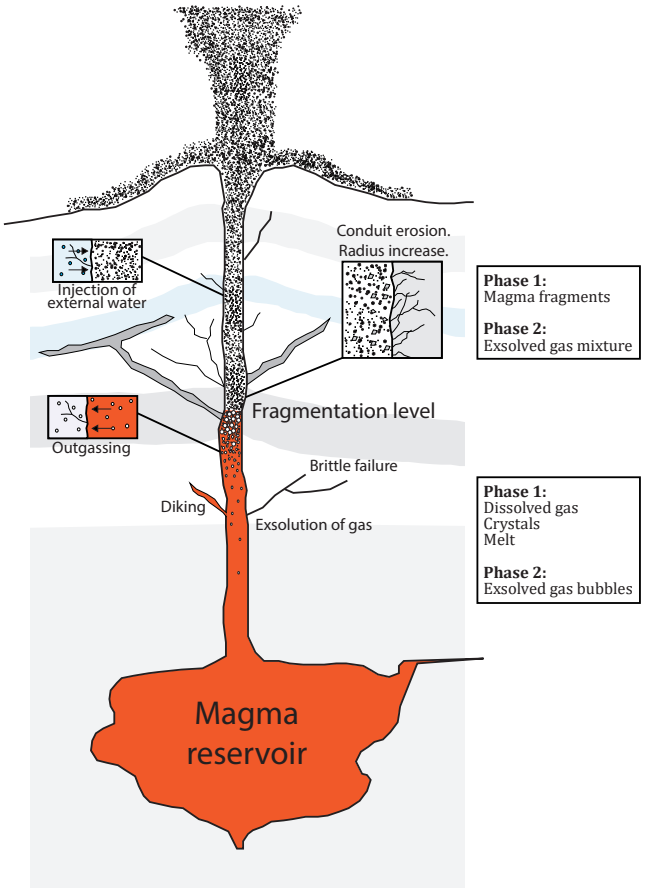

Figure 1: Schematic illustration of volcanic conduits.

$$T_i = \frac{\partial e_i}{\partial s_i} \tag{2}$$

The model includes the conservation laws of total mass (Eq. 3), momentum (Eq. 4) and energy (Eq. 5).

$$\frac{\partial}{\partial z}\left(\rho u R_{eq}^2\right) = -2J_{lat} f_{\epsilon_1} R_{eq} \tag{3}$$

$$\begin{aligned}\frac{\partial}{\partial z}\Big(\Big(\alpha_1(\rho_1 u_1^2 + p_1) + \alpha_2(\rho_2 u_2^2 + p_2)\Big) R_{eq}^2\Big) \\ = -\rho g R_{eq}^2 - 2J_{lat} f_{\epsilon_1} u_2 R_{eq} - \frac{8\chi_1 \mu u_1}{f_{\epsilon_2}^2} - \frac{\chi_2 \lambda_w \rho_2 u_2^2 R_{eq}}{4 f_{\epsilon_2}^2}\end{aligned} \tag{4}$$

$$\frac{\partial}{\partial z}\Bigg(\Bigg(\alpha_1\rho_1 u_1\left(e_1+\frac{p_1}{\rho_1}+\frac{u_1^2}{2}\right)+\alpha_2\rho_2 u_2\left(e_2+\frac{p_2}{\rho_2}+\frac{u_2^2}{2}\right)$$
$$-\rho x_1 x_2(u_1-u_2)(s_1-s_2)T\Bigg)R_{eq}^2\Bigg)=-\rho g u R_{eq}^2-\frac{8\chi_1\mu u_1^2}{f_{\epsilon_2}^2} \tag{5}$$
$$-\frac{\chi_2\lambda_w\rho_2 u_2^3 R_{eq}}{4f_{\epsilon_2}^2}-2J_{lat}f_{\epsilon_1}\left(c_g T+\frac{u_2^2}{2}\right)R_{eq}$$

where z is the vertical coordinate, ρ is mixture density, u is mixture velocity, R_{eq} is the equivalent conduit radius (Eq. 6), J_{lat} is the lateral gas flux through conduit walls, f_{ϵ_1} is a conduit eccentricity-derived factor (Eq. 7), g is the acceleration of gravity, χ_i controls the inclusion of wall friction (1 or 0, function of the continuous phase index), μ is mixture viscosity, f_{ϵ_2} is an additional conduit eccentricity-derived factor (Eq. 8), λ_w is a drag coefficient [3], x_i is the mass fraction of phase i, T is mixture temperature and c_g is the specific heat capacity of exsolved gas.

$$R_{eq}=\sqrt{R_a\cdot R_b} \tag{6}$$

$$f_{\epsilon_1}=\frac{3(1+\sqrt{1-\epsilon^2})-\sqrt{(3+\sqrt{1-\epsilon^2})\cdot(1+3\sqrt{1-\epsilon^2})}}{2\cdot\sqrt[4]{1-\epsilon^2}} \tag{7}$$

$$f_{\epsilon_2}=\sqrt{\frac{2\sqrt{1-\epsilon^2}}{2-\epsilon^2}} \tag{8}$$

where R_a is the maximum semi-axis, R_b is the minimum semi-axis and ϵ is conduit eccentricity (Eq. 9).

$$\epsilon=\sqrt{1-\frac{R_b^2}{R_a^2}} \tag{9}$$

Phase 1 volume fraction is governed by the following equation:

$$\frac{\partial}{\partial z}\left(\rho u\alpha_1 R_{eq}^2\right)=-\frac{1}{\tau^{(p)}}(p_2-p_1)R_{eq}^2 \tag{10}$$

where $\tau^{(p)}$ is the relaxation parameter which controls the pressure difference between both phases ($[\mathrm{m}^2/\mathrm{s}]$).

Furthermore, the model includes an additional equation for controlling the relative velocity between the phases:

$$\frac{\partial}{\partial z}\left(\left(\frac{u_1^2}{2}-\frac{u_2^2}{2}+e_1-e_2+\frac{p_1}{\rho_1}-\frac{p_2}{\rho_2}-(s_1-s_2)T\right)R_{eq}^2\right) = -\frac{8\chi_1\mu u_1}{\alpha_1\rho_1 f_{\epsilon_2}^2}+\frac{\chi_2\lambda_w u_2^2 R_{eq}}{4\alpha_2 f_{\epsilon_2}^2}-\frac{\rho}{\rho_1\rho_2}\delta_f(u_1-u_2)R_{eq}^2 \tag{11}$$

where δ_f is the drag factor ($[\mathrm{kg/m^3 s}]$).

Finally, the system of equations presents the mass conservation laws of crystals (Eq. 12), dissolved water (Eq. 13) and exsolved gas (Eq. 14).

$$\frac{\partial}{\partial z}\left(\alpha_1\rho_c\alpha_c u_1 R_{eq}^2\right) = -\frac{1}{\tau^{(c)}}\alpha_1\rho_c(\alpha_c-\alpha_c^{eq})R_{eq}^2 \tag{12}$$

$$\frac{\partial}{\partial z}\left(x_d\alpha_1\left(\rho_1-\alpha_c\rho_c\right)u_1 R_{eq}^2\right) = -\frac{(x_d-x_d^{eq})}{\tau^{(d)}}\alpha_1\left(\rho_1-\alpha_c\rho_c\right)R_{eq}^2 \tag{13}$$

$$\frac{\partial}{\partial z}\left(\alpha_g\rho_g u_2 R_{eq}^2\right) = -2J_{lat}f_{\epsilon_1}R_{eq}+\frac{(x_d-x_d^{eq})}{\tau^{(d)}}\alpha_1\left(\rho_1-\alpha_c\rho_c\right)R_{eq}^2 \tag{14}$$

where ρ_c is density of crystals, α_c is the volume fraction of crystals in phase 1, $\tau^{(c)}$ is the crystallization relaxation parameter ([s]), α_c^{eq} is the equilibrium value of α_c, x_d is the mass fraction of dissolved water in the phase composed by melt and dissolved gas, $\tau^{(d)}$ is the relaxation parameter which controls the exsolution rate of water ([s]), x_d^{eq} is the equilibrium value of x_d, while α_g and ρ_g are volume fraction and density of exsolved gas.

For the model solution, it employs a numerical shooting technique: for a given inlet pressure, the model adjusts the inlet flow rate until the appropriate boundary condition (choked flow or atmospheric pressure) is reached. For the spatial integration of the equations, a well-established PI step-size control technique is adopted, with the relaxation terms treated implicitly to guarantee the stability of the numerical scheme.

2 Constitutive equations

In order to offer the possibility of describing the behaviour of a wide range of magma compositions and volcanic phenomena, a complete set of constitutive equations has been implemented in the code.

Table 1: Available models for calculating $\theta_c(\alpha_c)$ in MAMMA.

Model	Equation	Auxiliary variables
None	$\theta_c = 1.0$	
Costa [4]	$\theta_c = \left(1 - c_1 \cdot \mathrm{erf}\left(\frac{\sqrt{\pi}}{2}\alpha_c\left(1 + \frac{c_2}{(1-\alpha_c)^{c_3}}\right)\right)\right)^{\frac{c_4}{c_1}}$	$c_1 = 0.9995$. $c_2 = 0.4$. $c_3 = 1.0$. $c_4 = -2.5$.
Dingwell [8]	$\theta_c = \left(1 + 0.75 \cdot \frac{\alpha_c}{c-\alpha_c}\right)^2$	$c = 0.84$
Lejeune-Richet [9]	$\theta_c = \left(1 - \frac{\alpha_c}{c_1}\right)^{-c_2}$	$c_1 = 0.7$. $c_2 = 3.4$.
Melnik-Sparks v1 [10]	$\log_{10}\left(\frac{\theta_c}{c_1}\right) = \mathrm{atan}(c_2 \cdot (\alpha_c - c_3)) + \frac{\pi}{2}$	$c_1 = 0.84$ ([1]). $c_2 = 20.6$. $c_3 = 0.62$.
Melnik-Sparks v2 [11]	$\log_{10}\left(\frac{\theta_c}{c_1}\right) = \mathrm{atan}(c_2 \cdot (\alpha_c - c_3)) + \frac{\pi}{2}$	$c_1 = 0.68$ ([1]). $c_2 = 8.6$. $c_3 = 0.69$.
Vona v1 [12]	$\theta_c = \frac{1+\phi^{c_2}}{\left(1-(1-c_3)\mathrm{erf}\left(\frac{\sqrt{\pi}}{2(1-c_3)}\phi(1+\phi^{c_4})\right)\right)^{c_1 c_5}}$	$\phi = \sum_j \alpha_{c_j}\rho_{c_j}/\rho_1 c_1$. $c_1 = 0.27$. $c_2 = 12.16$. $c_3 = 0.032$. $c_4 = 0.84$. $c_5 = 2.8$.
Vona v2 [12]	$\theta_c = \frac{1+\phi^{c_2}}{\left(1-(1-c_3)\mathrm{erf}\left(\frac{\sqrt{\pi}}{2(1-c_3)}\phi(1+\phi^{c_4})\right)\right)^{c_1 c_5}}$	$\phi = \sum_j \alpha_{c_j}\rho_{c_j}/\rho_1 c_1$. $c_1 = 0.39$. $c_2 = 1.16$. $c_3 = 0.03$. $c_4 = 0.84$. $c_5 = 2.8$.

([1]) Modified for producing $\theta_c(0) = 1.0$.

2.1 Viscosity models

Since it has been suggested a strong effect of crystal content [4, 5, 6] and exsolved gas bubbles [5, 7] on the resulting mixture rheology, magma viscosity (μ) is evaluated using the following expression:

$$\mu = \mu_{melt} \cdot \theta_c(\alpha_c) \cdot \theta_g(\alpha_g) \tag{15}$$

where μ_{melt} is the crystal and bubble-free viscosity; whereas $\theta_c(\alpha_c)$ and $\theta_g(\alpha_g)$ account for the effect of crystals and bubbles on the resulting viscosity, respectively.

The following models are implemented for calculating μ_{melt}, while the available expressions for calculating θ_c and θ_g are shown in Tables 1 and 2 and Figs. 2 and 3.

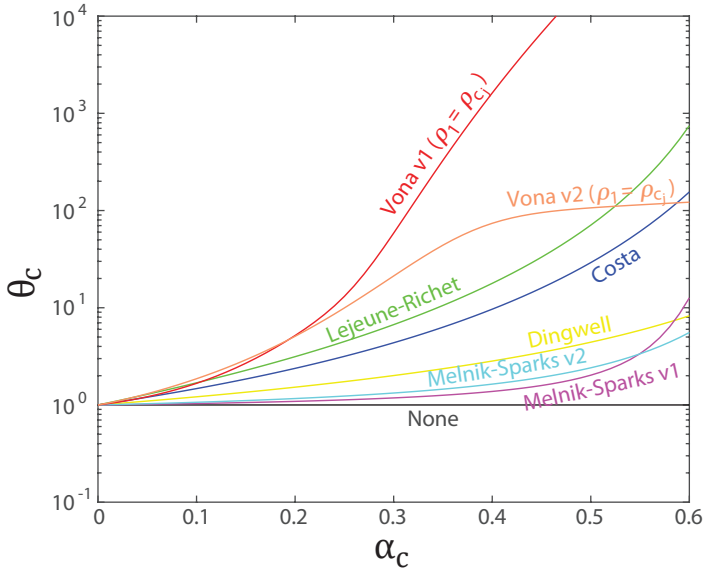

Figure 2: Available models for calculating $\theta_c(\alpha_c)$ in MAMMA.

2.1.1 Hess and Dingwell [24]

This model is based on a multiple non-linear regression of 111 measurements of viscosity, and is adapted for studying rhyolitic magmas:

$$\log_{10}(\mu_{melt}) = -3.545 + 0.833 \cdot \ln(\mathrm{w}) + \frac{9601 - 2368 \cdot \ln(\mathrm{w})}{T - (195.7 + 32.25 \cdot \ln(\mathrm{w}))} \tag{16}$$

where μ_{melt} is expressed in $\mathrm{Pa} \cdot \mathrm{s}$, w is dissolved water concentration in $\mathrm{wt.\%}$ and T is temperature in K.

2.1.2 Giordano et al. [25]

This model predicts the non-Arrhenian Newtonian viscosity of silicate melts as a function of T and melt composition (major elements). Melt viscosity (μ_{melt}) is calculated using:

$$\log_{10}(\mu_{melt}) = -4.55 + \frac{B_G}{T - C_G} \tag{17}$$

where B_G and C_G are composition-dependent constants (Eq. 18 and Eq. 19, respectively).

$$B_G = \sum_{i=1}^{7}(b_i M_i) + \sum_{j=1}^{3} b_{1j} M_{1j} \tag{18}$$

Table 2: Available models for calculating $\theta_g(\alpha_g)$ in MAMMA.

Model	Equation	Auxiliary variables
None	$\theta_g = 1.0$	
Bagdassarov-Dingwell [13]	$\theta_g = \frac{1}{1+b\cdot\alpha_g}$	$b = 22.4$
Costa et al. [14]	$\theta_g = \frac{1+25\cdot \mathrm{Ca}^2(1-\alpha_g)^{8/3}}{(1-\alpha_g)\cdot(1+25\cdot \mathrm{Ca}^2)}$	Ca ([1])
Ducamp-Raj [15]	$\theta_g = \exp\left(\frac{b\cdot\alpha_g}{1-\alpha_g}\right)$	$b = -3$
Eilers [16, 17]	$\theta_g = \left(1+\frac{1.25\alpha_g}{1-b\cdot\alpha_g}\right)^2$	$b = 1.29$
Mackenzie [18]	$\theta_g = 1-\frac{5}{3}\alpha_g$	
Quane-Russel [19]	$\theta_g = \exp\left(\frac{b\cdot\alpha_g}{1-\alpha_g}\right)$	$b = -0.63$ ([2])
Rahaman [20]	$\theta_g = \exp(-b\cdot\alpha_g)$	$b = 11.2$
Sibree [21]	$\theta_g = \frac{1}{1-(b\cdot\alpha_g)^{1/3}}$	$b = 1.2$
Taylor [22]	$\theta_g = 1+\alpha_g$	

([1]) Capillarity number. Calculated following Llewellin and Manga [23].
([2]) Adapted for Phlegrean Fields.

$$C_G = \sum_{i=1}^{6}(c_i N_i) + c_{11}N_{11} \tag{19}$$

where M_i, M_{1j}, N_i and N_{11} refer to the combinations of $\mathrm{mol}\%$ oxides reported in Table 3, and b_i, b_{1j}, c_i and c_{11} are constant values (Table 3).

2.1.3 Whittington et al. [26]

In this case, the viscosity model is adapted to dacitic magmas and uses the following formulation:

$$\log_{10}(\mu_{melt}) = -4.43 + \frac{7618.3 - 17.25\cdot\log_{10}(\mathrm{w}+0.26)}{T-(406.1-292.6\cdot\log_{10}(\mathrm{w}+0.26))} \tag{20}$$

2.2 Solubility models

2.2.1 Henry's law

The equilibrium value of dissolved water is calculated using the following expression:

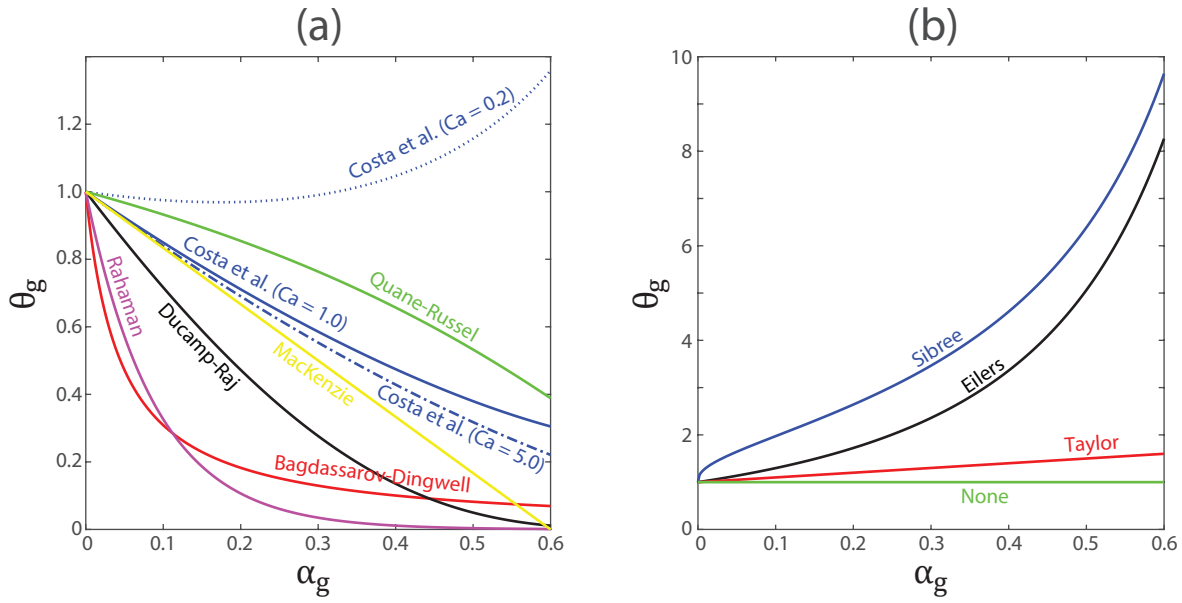

Figure 3: Available models for calculating $\theta_g(\alpha_g)$ in MAMMA.

$$x_d^{eq} = \sigma \left(\frac{p_g}{p_r} \right)^{\epsilon} \tag{21}$$

where σ is the solubility coefficient, p_g is pressure of the gas component, p_r is a reference value of pressure (equal to 1 [Pa]) and ϵ is the solubility exponent.

2.2.2 Polynomial fit

When the polynomial fit is employed, x_d^{eq} is computed with the following expression:

$$x_d^{eq} = c_1 \cdot \left(\frac{p_g}{p_r} \right)^2 + c_2 \cdot \left(\frac{p_g}{p_r} \right) \tag{22}$$

where c_1 and c_2 are fitting parameters.

2.3 Crystallization models

The equilibrium volume fraction of crystals (α_c^{eq}) is calculated using a polynomial fit, as described in Table 4.

Table 3: Coefficients for calculation of B_G and C_G from melt composition ($\mathrm{mol\%}$ oxide) [25].

Coefficient	Value	Oxides
b_1	159.6	$M_1 = \mathrm{SiO_2} + \mathrm{TiO_2}$
b_2	-173.3	$M_2 = \mathrm{Al_2O_3}$
b_3	72.1	$M_3 = \mathrm{FeO(T)} + \mathrm{MnO} + \mathrm{P_2O_5}$
b_4	75.7	$M_4 = \mathrm{MgO}$
b_5	-39.0	$M_5 = \mathrm{CaO}$
b_6	-84.1	$M_6 = \mathrm{Na_2O} + \mathrm{V}(^1)$
b_7	141.5	$M_7 = \mathrm{V} + \ln(1 + \mathrm{H_2O})$
b_{11}	-2.43	$M_{11} = (\mathrm{SiO_2}{+}\mathrm{TiO_2}) \cdot (\mathrm{FM}(^2))$
b_{12}	-0.91	$M_{12} = (\mathrm{SiO_2}{+}\mathrm{TA}(^3) + \mathrm{P_2O_5}) \cdot (\mathrm{NK}(^4) + \mathrm{H_2O})$
b_{13}	17.6	$M_{13} = (\mathrm{Al_2O_3}) \cdot (\mathrm{NK})$
c_1	2.75	$N_1 = \mathrm{SiO_2}$
c_2	15.7	$N_2 = \mathrm{TA}$
c_3	8.3	$N_3 = \mathrm{FM}$
c_4	10.2	$N_4 = \mathrm{CaO}$
c_5	-12.3	$N_5 = \mathrm{NK}$
c_6	-99.5	$N_6 = \ln(1 + \mathrm{V})$
c_{11}	0.30	$N_{11} = (\mathrm{Al_2O_3}{+}\mathrm{FM} + \mathrm{CaO} - \mathrm{P_2O_5}) \cdot (\mathrm{NK} + \mathrm{V})$

(^{1}) $\mathrm{V} = \mathrm{H_2O} + \mathrm{F_2O_{-1}}$.
(^{2}) $\mathrm{FM} = \mathrm{FeO(T)} + \mathrm{MnO} + \mathrm{MgO}$.
(^{3}) $\mathrm{TA} = \mathrm{TiO_2}{+}\mathrm{Al_2O_3}$.
(^{4}) $\mathrm{NK} = \mathrm{Na_2O} + \mathrm{K_2O}$.

2.4 Outgassing models

2.4.1 Forchheimer's law [3]

The model is dependent on the relative position of the fragmentation level. Below magma fragmentation, since a non-linear relationship between pressure gradient and gas flow rate has been recognized, Degruyter et al. [3] describe the outgassing process using the Forchheimer's law, which includes the influence of viscous (linear term) and inertial forces (quadratic term) (Eq. 23). Above magma fragmentation, the model presented by Yoshida and Koyaguchi [27] is considered; and the presence of a transitional domain is also assumed (Eq. 23). Please note that $|dp/dz| = \delta_f \cdot \triangle u$, where $\triangle u$ is the velocity difference between both phases.

$$\left|\frac{dp}{dz}\right| = \begin{cases} \frac{\mu_g}{k_D}(\triangle u) + \frac{\rho_g}{k_I}(\triangle u)^2 & \text{if } \alpha_g \leq \alpha_{cr} \\ \left(\frac{\mu_g}{k_D}(\triangle u) + \frac{\rho_g}{k_I}(\triangle u)^2\right)^{1-t} \cdot \left(\frac{3C_D}{8r_a}\rho_g(\triangle u)^2\right)^t & \text{if } \alpha_{cr} < \alpha_g < \alpha_t \\ \frac{3C_D}{8r_a}\rho_g(\triangle u)^2 & \text{if } \alpha_g \geq \alpha_t \end{cases} \tag{23}$$

where μ_g and ρ_g are viscosity and density of the exsolved gas phase, k_D and k_I are the Darcian and inertial permeabilities, respectively (Eq. 24 and Eq. 25), C_D is a drag coefficient, r_a is the average size of the fragmented magma particles, $t = (\alpha_g - \alpha_{cr})/(\alpha_t - \alpha_{cr})$ and α_t controls the range of the transitional domain.

$$k_D = \frac{(f_{rb} r_b)^2}{8} \alpha_g^m \tag{24}$$

$$k_I = \frac{f_{rb} r_b}{f} \alpha_g^{(1+3m)/2} \tag{25}$$

$$r_b = \left(\frac{\alpha_g}{\frac{4\pi}{3} N_{bd} \alpha_1}\right)^{1/3} \tag{26}$$

where f_{rb} is the throat-bubble size ratio, r_b is the average bubble size, N_{bd} is the bubble density number and f and m are fitting parameters.

2.4.2 Darcy's law

In this case, the inertial forces below magma fragmentation (quadratic term) and the transitional domain are not considered, and thus the resulting model is described by the following expression:

$$\left|\frac{dp}{dz}\right| = \begin{cases} \frac{\mu_g}{k_D}(\triangle u) & \text{if } \alpha_g \leq \alpha_{cr} \\ \frac{3C_D}{8r_a}\rho_g(\triangle u)^2 & \text{if } \alpha_g > \alpha_{cr} \end{cases} \tag{27}$$

2.5 Degassing model

If lateral degassing is considered, it follows Eq. 28.

$$J_{lat} = \frac{\rho_g \alpha_g k_{cr}}{\mu_g f_{\epsilon_2}} \frac{\partial p}{\partial r}\Big|_{r=R_{eq}} \tag{28}$$

where k_{cr} is country rock permeability.

2.6 Equations of state

In order to define the specific internal energy and entropy of melt, crystals and dissolved gas, a linearized version of the Mie-Gruneisen equation of state [28] was adopted:

$$e_l(\rho_l, T) = \bar{e}_l + c_{v,l}T + \frac{\rho_{0,l}C_{0,l}^2 - \gamma_l p_{0,l}}{\gamma_l \rho_l} \tag{29}$$

$$s_l(\rho_l, T) = s_{0,l} + c_{v,l} \cdot \ln\left(\frac{T}{T_{0,l}}\left(\frac{\rho_{0,l}}{\rho_l}\right)^{\gamma_l - 1}\right) \tag{30}$$

where $\bar{e}_l$ is formation energy, $c_{v,l}$ is the specific heat capacity at constant volume, $\rho_{0,l}$ and $C_{0,l}$ are density and sound speed at a reference state, γ_l is the adiabatic exponent and $p_{0,l}$, $s_{0,l}$ and $T_{0,l}$ are pressure, specific entropy and temperature at a reference state. Subscript l refers to melt (m), the dissolved water (d) or crystals (c).

For the equation of state of exsolved gas, two models are available:

2.6.1 Ideal gas

The internal energy and specific entropy are calculated using equations 31 and 32, respectively.

$$e_g(\rho_g, T) = \bar{e}_g + c_{v,g}T \tag{31}$$

$$s_g(\rho_g, T) = s_{0,g} + c_{v,g} \cdot \ln\left(\frac{T}{T_{0,g}}\left(\frac{\rho_{0,g}}{\rho_g}\right)^{\gamma_g - 1}\right) \tag{32}$$

where $c_{v,g}$ is the specific heat capacity at constant volume, $\bar{e}_g$ is the formation energy, $s_{0,g}$, $T_{0,g}$ and $\rho_{0,g}$ are specific entropy, temperature and density at a reference state and γ_g is the adiabatic exponent.

2.6.2 Van der Waals

In this case, the following equations are employed:

$$e_g(\rho_g, T) = \bar{e}_g + c_{v,g}T - a_g \cdot \rho_g \tag{33}$$

$$s_g(\rho_g, T) = s_{0,g} + c_{v,g} \cdot \ln\left(\frac{T}{T_{0,g}}\left(\frac{\rho_{0,g}}{\rho_g} \cdot (1 - b_g \cdot \rho_g)\right)^{\gamma_g - 1}\right) \tag{34}$$

where:

$$a_g = \frac{27}{64} \cdot \frac{c_{v,g}^2(\gamma_g - 1)^2 T_{cr,g}^2}{p_{cr,g}} \tag{35}$$

$$b_g = \frac{1}{8} \cdot \frac{c_{v,g}(\gamma_g - 1) T_{cr,g}}{p_{cr,g}} \tag{36}$$

where $T_{cr,g}$ and $p_{cr,g}$ are critical temperature and pressure of water.

3 vhub app

The user-friendly version of MAMMA allows to model conduit dynamics for six magma compositions (rhyolitic, dacitic, trachytic, phonolitic, andesitic and basaltic), considering three different simulation modalities. Fig. 4 presents the user interface, where the following input parameters must be imposed:

(1) Simulation type (choice): it indicates the simulation modality. Three alternatives are available:

(a) **Modality 1**: Impose conduit geometry (single simulation). In this case, a single simulation is performed, considering the magma properties and the conduit geometry set by the user. Mass discharge rate is an output parameter of this simulation.

(b) **Modality 2**: Impose MDR (single simulation). A set of numerical simulations is performed in order to compute the conduit dimensions able to produce the mass discharge rate set by the user. Magma properties (i.e. water content, temperature, overpressure) are input parameters, while input conduit radius is employed as an initial guess for conduit dimensions. Here, cylindrical conduits are considered.

(c) **Modality 3**: Impose conduit geometry with uncertainty ranges. A set of numerical simulations is performed with some variable input parameters (water

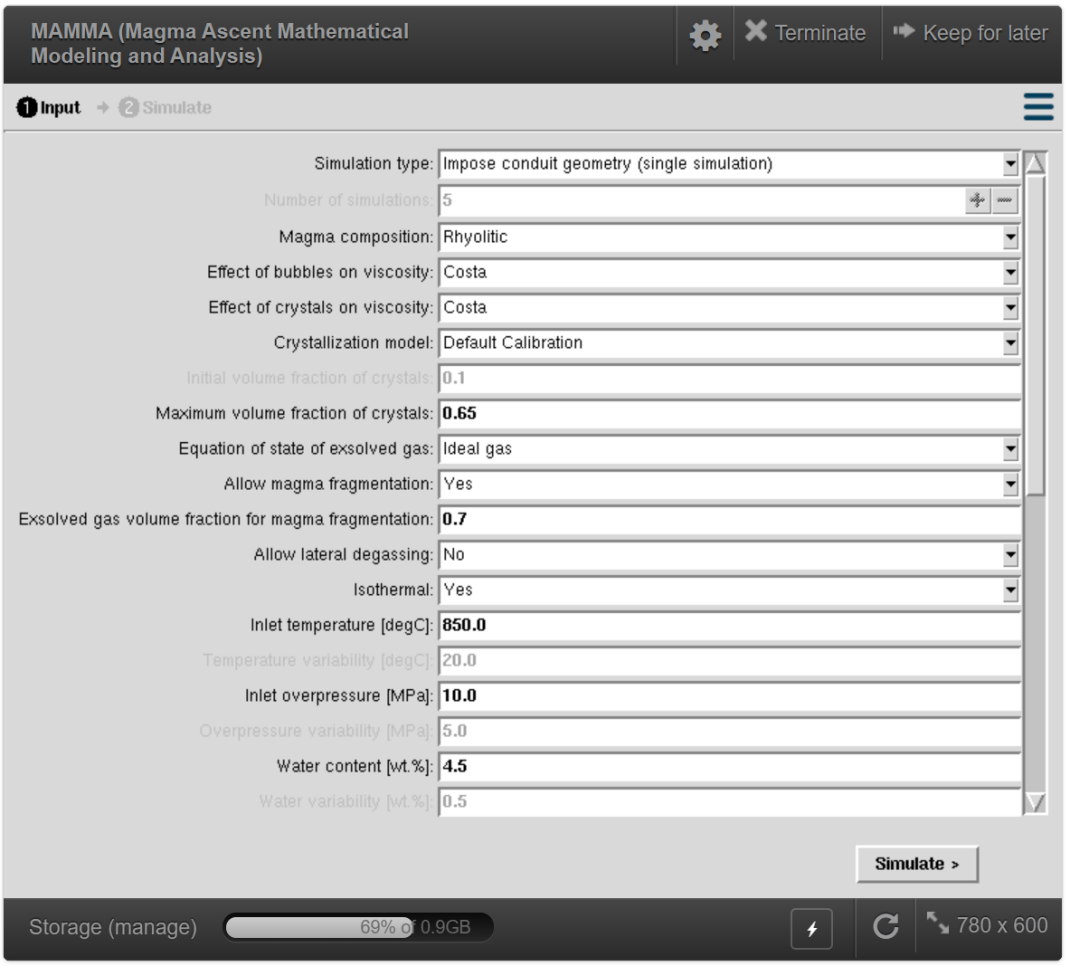

Figure 4: User interface.

content, overpressure, temperature and conduit radius), as a function of the variability ranges defined by the user. The total number of simulations is defined by the user, allowing to estimate the variability of some output parameters considering the uncertainty of model inputs. Also in this case, cylindrical conduits are considered. The use of test simulations with modality 1 is highly recommended before launching a large number of simulations, in order to test the adopted ranges of input parameters.

(2) Number of simulations (number): only employed when Modality 3 is selected.

(3) Magma composition (choice): rhyolitic, dacitic, trachytic, phonolitic, andesitic or basaltic. It determines the following models and default parameters:

(a) Magma viscosity (Hess and Dingwell et al. [24] for rhyolitic magmas; Whittington et al. [26] for dacitic magmas, and Giordano et al. [25] for trachytic, phonolitic, andesitic and basaltic melts, which depends on the adopted magma composition).

(b) Water solubility (Zhang [29] for rhyolitic magmas, Moore et al. [30] for dacitic magmas, Di Matteo et al. [31] for trachytic magmas, Carroll and Blank [32] for phonolitic melts, Borcharnikov et al. [33] for andesitic magmas and Dixon et al. [34] for basaltic magmas).

(c) Magma composition (sample Ch-1-08 [35] for rhyolitic magmas, sample 27-1a-86 [36] for dacitic magmas, sample ZAC [31] for trachytic magmas, sample T2-182 [32] for phonolitic magmas, sample 27-1b-86 [36] for andesitic magmas and sample VI-31 [37] for basaltic magmas). These values were employed for calibrating crystallization models and, when it is required, for viscosity models.

(d) Crystallization (if it is considered). Using a set of alphaMELTS [38] simulations for different conditions of pressure, temperature and water content, we calibrated a crystallization model for each magma composition. The resulting expressions for calculating the mass fraction of crystals are presented in Table 4.

(e) Several additional default parameters (see Tables 5 and 6). These parameters allow to model outgassing processes and the equations of state of crystals, melt, bubbles and dissolved water.

(4) Effect of bubbles on viscosity (choice): Bagdassarov - Dingwell [13], Costa [14], Ducamp - Raj [15], Eilers [16, 17], MacKenzie [18], None, Quane - Russel [19], Rahaman [20], Sibree [21] or Taylor [22].

(5) Effect of crystals on viscosity (choice): Costa [4], Dingwell [8], Lejeune - Richet [9], Melnik-Sparks v1 [10], Melnik-Sparks v2 [11], None, Vona v1 [12] or Vona v2 [12].

(6) Crystallization model (choice): Default calibration or None.

(7) Initial volume fraction of crystals (number): it represents the volume fraction of crystals at conduit bottom. It is only employed when Crystallization model is equal to

Table 4: Calibrated crystallization models. The expression for calculating crystal mass fraction is: $x_c^l = d_{T2} \cdot T^2 + d_T \cdot T + d_p \cdot p + d_w \cdot \mathrm{w} + d_0$, where T is temperature in K, p is pressure in Pa and w is water content in wt.%.

Parameter	Rhyolitic	Dacitic	Trachytic	Phonolitic	Andesitic	Basaltic
d_{T2}	$5.17 \cdot 10^{-6}$	$2.72 \cdot 10^{-7}$	$-4.47 \cdot 10^{-7}$	$1.02 \cdot 10^{-5}$	$-2.25 \cdot 10^{-6}$	$3.52 \cdot 10^{-6}$
d_T	$-1.29 \cdot 10^{-2}$	$-2.22 \cdot 10^{-3}$	$-2.29 \cdot 10^{-3}$	$-2.78 \cdot 10^{-2}$	$3.52 \cdot 10^{-3}$	$-1.13 \cdot 10^{-2}$
d_p	$2.08 \cdot 10^{-10}$	$1.89 \cdot 10^{-10}$	$4.13 \cdot 10^{-10}$	$3.30 \cdot 10^{-10}$	$1.92 \cdot 10^{-10}$	$1.69 \cdot 10^{-10}$
d_w	-7.04	-7.67	-12.06	-7.65	-9.28	-6.14
d_0	8.31	2.69	4.01	18.95	-0.33	9.09

The ranges of input parameters used in alphaMELTS [38] simulations are:
Rhyolitic magmas: $T = 1023.15$ - 1223.15 K, $p = 0$ - 250 MPa, w $= 0$ - 6 wt.% (R $= 0.92$).
Dacitic magmas: $T = 1023.15$ - 1223.15 K, $p = 0$ - 250 MPa, w $= 0$ - 6 wt.% (R $= 0.99$).
Trachytic magmas: $T = 1073.15$ - 1273.15 K, $p = 0$ - 250 MPa, w $= 0$ - 5 wt.% (R $= 0.96$).
Phonolitic magmas: $T = 1073.15$ - 1273.15 K, $p = 0$ - 250 MPa, w $= 0$ - 5 wt.% (R $= 0.96$).
Andesitic magmas: $T = 1173.15$ - 1473.15 K, $p = 0$ - 250 MPa, w $= 0$ - 4 wt.% (R $= 0.98$).
Basaltic magmas: $T = 1173.15$ - 1473.15 K, $p = 0$ - 250 MPa, w $= 0$ - 4 wt.% (R $= 0.97$).

None. Otherwise, the inlet content of crystals is equal to the equilibrium value at conduit bottom.

(8) Maximum volume fraction of crystals (number): it represents the maximum volume fraction of crystals allowed by the code. It is only employed when Crystallization model is equal to Default calibration.

(9) Equation of state of exsolved gas (choice): Ideal gas or Van der Waals.

(10) Allow magma fragmentation (choice).

(11) Exsolved gas volume fraction for magma fragmentation (number): it is only employed when magma fragmentation is allowed and represents the critical volume fraction of bubbles for fragmentation.

(12) Allow lateral degassing (choice).

(13) Isothermal (choice).

(14) Inlet temperature (number): Temperature at conduit bottom.

(15) Temperature variability (number): Measure of temperature uncertainty. It is only employed when the Modality 3 is selected.

(16) Inlet overpressure (number): Overpressure at conduit bottom. For computing inlet pressure, it is assumed a default country rock density of 2700 kg/m^3.

(17) Overpressure variability (number): Measure of overpressure uncertainty. It is only employed when the Modality 3 is selected.

(18) Water content (number): total water content at conduit bottom.

(19) Water content variability (number): Measure of water content uncertainty. It is only employed when the Modality 3 is selected.

(20) Conduit geometry (choice): Cylinder, Dyke, Depth dependent 1 (linearly enlarging conduit), Depth dependent 2 (cylindrical lower portion and linearly enlarging upper portion) or Depth dependent 3 (two cylindrical portions connected by a transitional, linearly enlarging zone) (Fig. 5). Cylindrical conduit is the only geometry available when Modalities 2 and 3 are selected (indeed, in that case, this field is disabled).

(21) Conduit length (number).

(22) Fixed radius (number): it is only employed when conduit geometry is equal to Cylinder. When Modality 2 is selected, this value is employed as a first guess of conduit dimensions.

(23) Radius variability (number): Measure of conduit radius uncertainty. It is only employed when the Modality 3 is selected.

(24) Major semi-axis (number): it is only employed when conduit geometry is equal to Dyke.

(25) Minor semi-axis (number): it is only employed when conduit geometry is equal to Dyke.

(26) Minimum radius (number): it is only employed when conduit geometry is equal to Depth dependent 1, Depth dependent 2 or Depth dependent 3.

(27) Maximum radius (number): it is only employed when conduit geometry is equal to Depth dependent 1, Depth dependent 2 or Depth dependent 3.

(28) Transition depth (number): it is only employed when conduit geometry is equal to Depth dependent 2 or Depth dependent 3.

(29) Length of transition zone (number): it is only employed when conduit geometry is equal to Depth dependent 3.

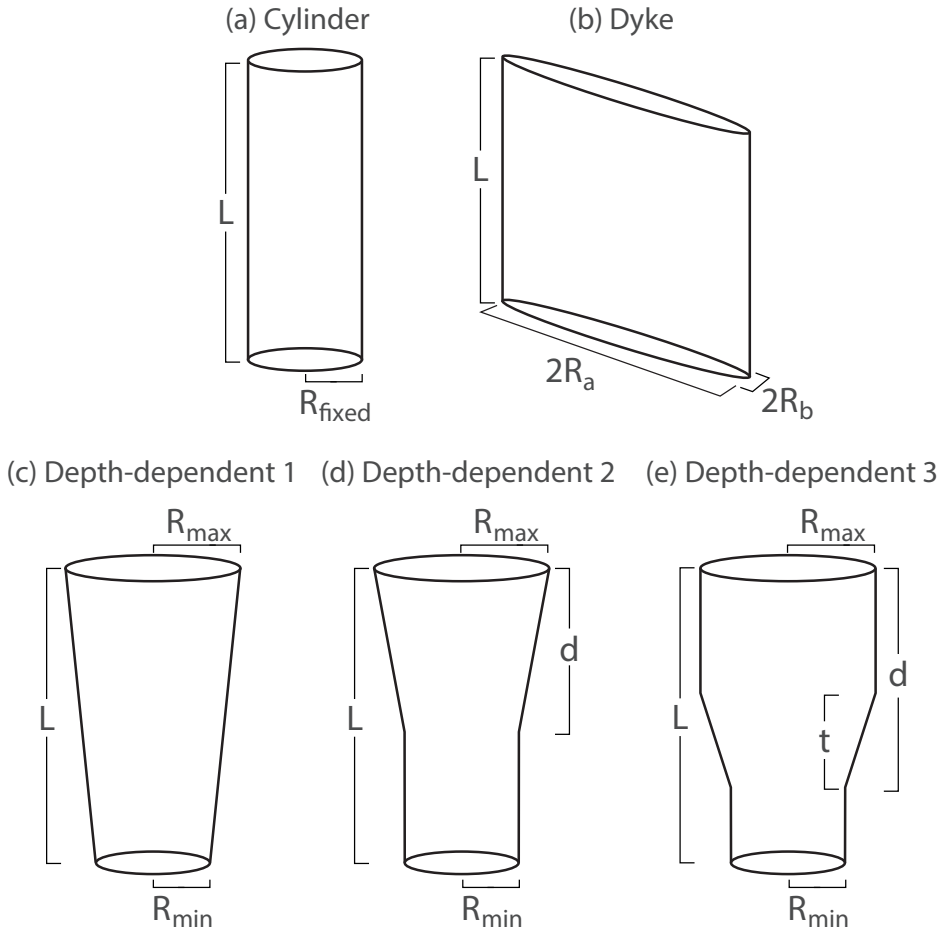

Figure 5: Available conduit geometries in the user-friendly version of MAMMA. L: conduit length. R_{fixed}: fixed radius. R_a: major semi-axis. R_b: minor semi-axis. R_{min}: minimum radius. R_{max}: maximum radius. d: transition depth. t: length of transition zone.

(30) Mass discharge rate (number): it is only employed when modality 2 is selected.

(31) Relaxation parameter for crystallization (number): $\log_{10}(\tau^{(c)})$.

(32) Relaxation parameter for exsolution of bubbles (number): $\log_{10}(\tau^{(d)})$.

(33) Relaxation parameter for pressure difference (number): $\log_{10}(\tau^{(p)})$.

(34) Outgassing model (choice): Forchheimer or Darcy.

(35) Average size of fragmented magma particles (number).

(36) Bubble number density (number).

The outputs of the model depend on the selected simulation modality. For modalities 1 and 2, model outputs are the profiles along the conduit of: (1) pressure (phase 1 and phase 2), (2) velocity (phase 1 and phase 2), (3) temperature, (4) dissolved water (actual and equilibrium value), (5) viscosity (mixture and melt), (6) density (phase 1 and phase 2), (7) crystal volume fraction (actual and equilibrium value), (8) exsolved gas volume fraction, (9) mass discharge rate, (10) equivalent radius and (11) solubility law (Fig. 6). A summary table is also included, with the most important eruptive parameters (mass discharge rate, exit velocity, exit pressure, exit density and fragmentation depth). Otherwise, for modality 3, model outputs are the frequency histograms of the following parameters: (1) mass discharge rate, (2) exit pressure, (3) exit velocity, (4) exit density, (5) fragmentation depth, (6) conduit radius (input parameter of each simulation), (7) temperature (input parameter of each simulation), (8) overpressure (input parameter of each simulation) and (9) water content (input parameter of each simulation). Also in this case, a summary table is included, which contains input and output parameters of each simulation. The input parameters of twelve test simulations are presented in Tables 7 and 8.

References

[1] E. Romenski, D. Drikakis, and E. Toro. "Conservative models and numerical methods for compressible two-phase flow". In: *Journal of Scientific Computing* 42.1 (2010), pp. 68–95.

[2] A. Starostin, A. Barmin, and O. Melnik. "A transient model for explosive and phreatomagmatic eruptions". In: *Journal of Volcanology and Geothermal Research* 143.1 (2005), pp. 133–151.

[3] W. Degruyter, O. Bachmann, A. Burgisser, and M. Manga. "The effects of outgassing on the transition between effusive and explosive silicic eruptions". In: *Earth and Planetary Science Letters* 349 (2012), pp. 161–170.

[4] A. Costa. "Viscosity of high crystal content melts: dependence on solid fraction". In: *Geophysical Research Letters* 32.22 (2005).

[5] H.M. Mader, E.W. Llewellin, and S.P. Mueller. "The rheology of two-phase magmas: A review and analysis". In: *Journal of Volcanology and Geothermal Research* 257.1 (2013), pp. 135–158.

[6] C. Cimarelli, A. Costa, S. Mueller, and H.M. Mader. "Rheology of magmas with bimodal crystal size and shape distributions: Insights from analog experiments". In: *Geochemistry, Geophysics, Geosystems* 12.7 (2011).

[7] M. Manga and M. Loewenberg. "Viscosity of magmas containing highly deformable bubbles". In: *Journal of Volcanology and Geothermal Research* 105.1 (2001), pp. 19–24.

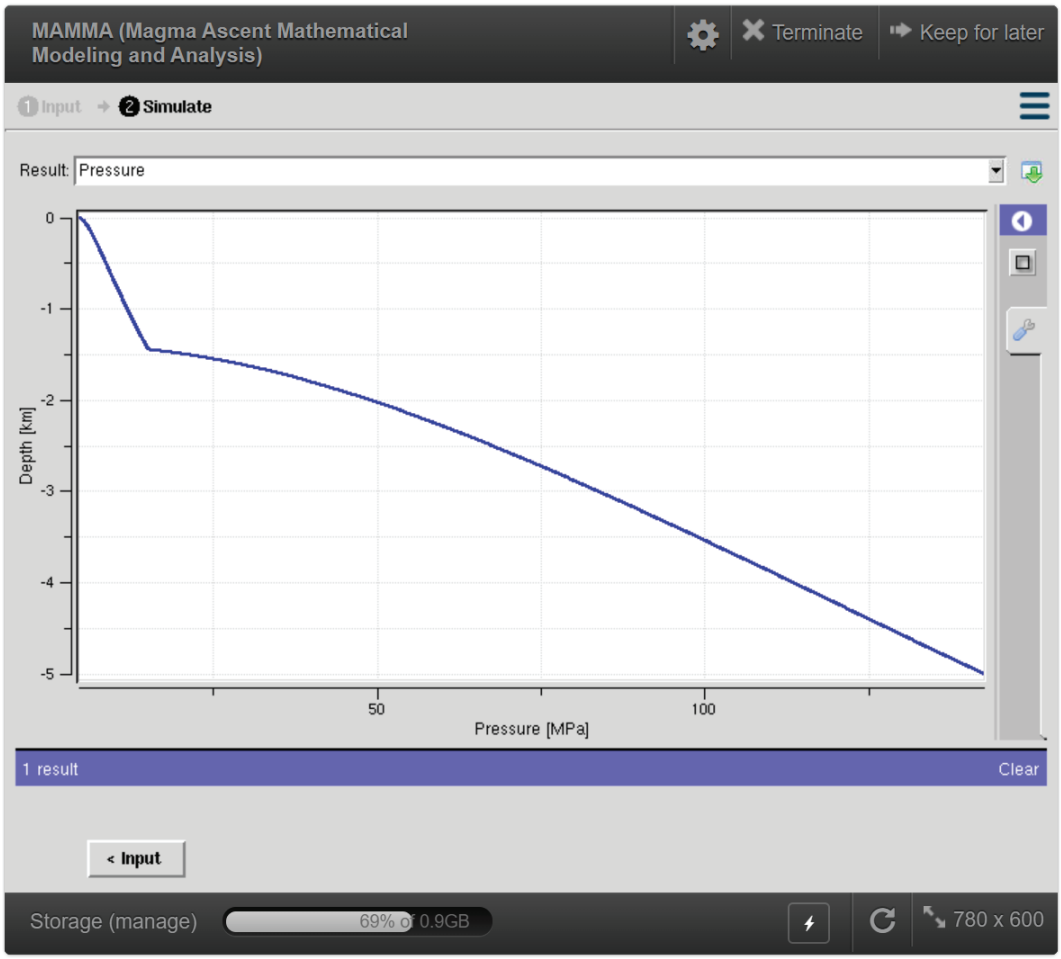

Figure 6: Results interface.

[8] D.B. Dingwell, N. Bagdassarov, G. Bussod, and S.L. Webb. "Magma rheology". In: *Mineralogical Association of Canada Short Course Handbook on Experiments at High Pressures and Application to the Earths Mantle* 21.1 (1993), pp. 131–196.

[9] A.M. Lejeune and P. Richet. "Rheology of crystal-bearing silicate melts: An experimental study at high viscosities". In: *Journal of Geophysical Research: Solid Earth* 100.B3 (1995), pp. 4215–4229.

[10] O. Melnik and R.S.J. Sparks. "Nonlinear dynamics of lava dome extrusion". In: *Nature* 402.6757 (1999), pp. 37–41.

[11] O. Melnik and R.S.J. Sparks. "Controls on conduit magma flow dynamics during lava dome building eruptions". In: *Journal of Geophysical Research: Solid Earth* 110.B2 (2005).

[12] A. Vona, C. Romano, D.B. Dingwell, and D. Giordano. "The rheology of crystal-bearing basaltic magmas from Stromboli and Etna". In: *Geochimica et Cosmochimica Acta* 75.11 (2011), pp. 3214–3236.

[13] N.S. Bagdassarov and D.B. Dingwell. “Frequency dependent rheology of vesicular rhyolite”. In: *Journal of Geophysical Research: Solid Earth* 98.B4 (1993), pp. 6477–6487.

[14] A. Costa, O. Melnik, and R.S.J. Sparks. “Controls of conduit geometry and wallrock elasticity on lava dome eruptions”. In: *Earth and Planetary Science Letters* 260.1 (2007), pp. 137–151.

[15] V.C. Ducamp and R. Raj. “Shear and densification of glass powder compacts”. In: *Journal of the American Ceramic Society* 72.5 (1989), pp. 798–804.

[16] H. Eilers. “Die viskosität von emulsionen hochviskoser stoffe als funktion der konzentration”. In: *Colloid & Polymer Science* 97.3 (1941), pp. 313–321.

[17] H. Eilers. “Die viskositäts-konzentrationsabhängigkeit kolloider systeme in organischen lösungsmitteln”. In: *Kolloid-Zeitschrift* 102.2 (1943), pp. 154–169.

[18] J.K. Mackenzie. “Elastic constants of a solid containing spherical holes”. In: *Proceedings of the Royal Society B* 63.1 (1950), pp. 2–11.

[19] S.L. Quane, J.K. Russell, and E.A. Friedlander. “Time scales of compaction in volcanic systems”. In: *Geology* 37.5 (2009), pp. 471–474.

[20] M.N. Rahaman, L. De Jonghe, G.W. Scherer, and R.J. Brook. “Creep and densification during sintering of glass powder compacts”. In: *Journal of the American Ceramic Society* 70.10 (1987), pp. 766–774.

[21] J.O. Sibree. “The viscosity of froth”. In: *Transactions of the Faraday Society* 30.1 (1934), pp. 325–331.

[22] G. Taylor. “The viscosity of a fluid containing small drops of another fluid”. In: *Proceedings of the Royal Society of London. Series A, Containing Papers of a Mathematical and Physical Character* 138.834 (1932), pp. 41–48.

[23] E.W. Llewellin and M. Manga. “Bubble suspension rheology and implications for conduit flow”. In: *Journal of Volcanology and Geothermal Research* 143.1 (2005), pp. 205–217.

[24] K.U. Hess and D. Dingwell. “Viscosities of hydrous leucogranitic melts: A non-Arrhenian model”. In: *American Mineralogist* 81.9-10 (1996), pp. 1297–1300.

[25] D. Giordano, J. Russell, and D. Dingwell. “Viscosity of magmatic liquids: a model”. In: *Earth and Planetary Science Letters* 271.1 (2008), pp. 123–134.

[26] A.G. Whittington, B.M. Hellwig, H. Behrens, B. Joachim, A. Stechern, and F. Vetere. “The viscosity of hydrous dacitic liquids: implications for the rheology of evolving silicic magmas”. In: *Bulletin of Volcanology* 71.2 (2009), pp. 185–199.

[27] S. Yoshida and T. Koyaguchi. “A new regime of volcanic eruption due to the relative motion between liquid and gas”. In: *Journal of Volcanology and Geothermal Research* 89.1 (1999), pp. 303–315.

[28] O. Le Métayer, J. Massoni, and R. Saurel. “Modelling evaporation fronts with reactive Riemann solvers”. In: *Journal of Computational Physics* 205.2 (2005), pp. 567–610.

[29] Y. Zhang. “H2O in rhyolitic glasses and melts: measurement, speciation, solubility, and diffusion”. In: *Reviews of Geophysics* 37.4 (1999), pp. 493–516.

[30] G. Moore, T. Vennemann, and I.S.E. Carmichael. “Solubility of water in magmas to 2 kbar”. In: *Geology* 23.12 (1995), pp. 1099–1102.

[31] V. Di Matteo, M.R. Carroll, H. Behrens, F. Vetere, and R.A. Brooker. "Water solubility in trachytic melts". In: *Chemical Geology* 213.1 (2004), pp. 187–196.

[32] M.R. Carroll and J.G. Blank. "The solubility of H2O in phonolitic melts". In: *American Mineralogist* 82.5-6 (1997), pp. 549–556.

[33] R.E. Botcharnikov, F. Holtz, and H. Behrens. "Solubility and fluid–melt partitioning of H2O and Cl in andesitic magmas as a function of pressure between 50 and 500 MPa". In: *Chemical Geology* 418 (2015), pp. 117–131.

[34] J.E. Dixon, E.M. Stolper, and J.R. Holloway. "An experimental study of water and carbon dioxide solubilities in mid-ocean ridge basaltic liquids. Part I: calibration and solubility models". In: *Journal of Petrology* 36.6 (1995), pp. 1607–1631.

[35] J.M. Castro and D.B. Dingwell. "Rapid ascent of rhyolitic magma at Chaitén volcano, Chile". In: *Nature* 461.7265 (2009), p. 780.

[36] M.J. Defant, L.F. Clark, R.H. Stewart, M.S. Drummond, J.Z. de Boer, R.C. Maury, H. Bellon, T.E. Jackson, and J.F. Restrepo. "Andesite and dacite genesis via contrasting processes: the geology and geochemistry of El Valle Volcano, Panama". In: *Contributions to Mineralogy and Petrology* 106.3 (1991), pp. 309–324.

[37] L. Gurioli, A.J.L. Harris, B.F. Houghton, M. Polacci, and M. Ripepe. "Textural and geophysical characterization of explosive basaltic activity at Villarrica volcano". In: *Journal of Geophysical Research: Solid Earth* 113.B8 (2008).

[38] P.M. Smith and P.D. Asimow. "Adiabat_1ph: A new public front-end to the MELTS, pMELTS, and pHMELTS models". In: *Geochemistry, Geophysics, Geosystems* 6.2 (2005).

Table 5: Default parameters used in the user-friendly version of MAMMA.

Parameter	Rhyolitic	Dacitic	Trachytic	Phonolitic	Andesitic	Basaltic
p_{out} [Pa] ([1])	101300	101300	101300	101300	101300	101300
$p_{cr,g}$ [Pa]	22064000	22064000	22064000	22064000	22064000	22064000
$T_{cr,g}$ [K]	647	647	647	647	647	647
$c_{v,g}$ [m^2/s^2K]	1571	1571	1571	1571	1571	1571
γ_g	1.29	1.29	1.29	1.29	1.29	1.29
$\rho_{0,g}$ [kg/m^3]	0.58846	0.58846	0.58846	0.58846	0.58846	0.58846
$T_{0,g}$ [K]	373	373	373	373	373	373
$\bar{e}_g$ [m^2/s^2]	0	0	0	0	0	0
$s_{0,g}$ [m^2/s^2K]	0	0	0	0	0	0
μ_g [$Pa \cdot s$]	$1.5 \cdot 10^{-5}$	$1.5 \cdot 10^{-5}$	$1.5 \cdot 10^{-5}$	$1.5 \cdot 10^{-5}$	$1.5 \cdot 10^{-5}$	$1.5 \cdot 10^{-5}$
$\rho_{0,d}$ [kg/m^3]	1000	1000	1000	1000	1000	1000
$C_{0,d}$ [m/s]	407.0225	407.0225	407.0225	407.0225	407.0225	407.0225
$c_{v,d}$ [m^2/s^2K]	3637.57878	3637.57878	3637.57878	3637.57878	3637.57878	3637.57878
γ_d	1.11	1.11	1.11	1.11	1.11	1.11
$p_{0,d}$ [Pa]	100000000	100000000	100000000	100000000	100000000	100000000
$\bar{e}_d$ [m^2/s^2]	0	0	0	0	0	0
$s_{0,d}$ [m^2/s^2K]	0	0	0	0	0	0
Solubility model	Henry	Henry	Polynomial	Polynomial	Henry	Henry
σ / c_1	$4.11 \cdot 10^{-6}$	$6.12 \cdot 10^{-6}$	$-1 \cdot 10^{-18}$	$-2 \cdot 10^{-18}$	$8.1 \cdot 10^{-9}$	$5.1 \cdot 10^{-7}$
ϵ / c_2	0.5	0.469	$6 \cdot 10^{-10}$	$6 \cdot 10^{-10}$	0.818	0.6
$\rho_{0,c}$ [kg/m^3]	2650	2650	2750	2750	2900	3050
$C_{0,c}$ [m/s]	2000	2000	2000	2000	2000	2000
$c_{v,c}$ [m^2/s^2K]	350	350	350	350	360	360
γ_c	3.4	3.4	3.4	3.4	3.4	3.4
$p_{0,c}$ [Pa]	250000000	250000000	250000000	250000000	250000000	250000000
$\bar{e}_c$ [m^2/s^2]	0	0	0	0	0	0
$s_{0,c}$ [m^2/s^2K]	0	0	0	0	0	0
$\rho_{0,m}$ [kg/m^3]	2300	2350	2450	2450	2500	2650
$C_{0,m}$ [m/s]	1500	1500	1500	1500	1500	1500

([1]) Pressure at conduit top (for non choked conditions).

Table 6: Default parameters used in the user-friendly version of MAMMA.

Parameter	Rhyolitic	Dacitic	Trachytic	Phonolitic	Andesitic	Basaltic
$c_{v,m}$ [m^2/s^2K]	640	688	688	702	702	707
γ_m	2.1	2.1	2.1	2.1	2.1	2.1
$p_{0,m}$ [Pa]	140000000	140000000	140000000	140000000	140000000	140000000
$\bar{e}_m$ [m^2/s^2]	0	0	0	0	0	0
$s_{0,m}$ [m^2/s^2K]	0	0	0	0	0	0
Viscosity model	Hess and Dingwell 1996	Whittington et al 2009	Giordano et al. 2008	Giordano et al. 2008	Giordano et al. 2008	Giordano et al. 2008
g [m/s^2]	9.81	9.81	9.81	9.81	9.81	9.81
$\log_{10}(k_{cr}$ [m^2])	-12	-12	-12	-12	-12	-12
m	4	4	4	4	4	4
f_{rb}	0.5	0.5	0.5	0.5	0.5	0.5
f	10	10	10	10	10	10
C_D	0.8	0.8	0.8	0.8	0.8	0.8
λ_w	0.03	0.03	0.03	0.03	0.03	0.03
SiO_2 [wt.%]	75.60	68.18	61.71	59.38	58.61	53.77
TiO_2 [wt.%]	0.14	0.28	0.45	0.66	0.60	1.71
Al_2O_3 [wt.%]	13.90	17.81	18.56	18.92	17.48	14.61
FeO [wt.%]	1.35	2.52	3.17	3.47	6.24	10.98
MnO [wt.%]	0.05	0.06	0.27	0.20	0.12	0.28
MgO [wt.%]	0.26	0.95	0.23	0.33	3.59	4.94
CaO [wt.%]	1.46	4.10	1.64	0.79	7.44	8.82
Na_2O [wt.%]	4.04	4.29	6.11	10.07	3.71	3.35
K_2O [wt.%]	2.93	1.53	7.09	5.55	1.67	0.89
P_2O_5 [wt.%]	0.06	0.10	0.02	0.07	0.21	0.40

Table 7: Test simulations.

Parameter	S1	S2	S3	S4	S5	S6
Simulation type (modality)	1	1	1	1	1	1
Number of simulations	NaN	NaN	NaN	NaN	NaN	NaN
Composition	Rhyolitic	Dacitic	Trachytic	Phonolitic	Andesitic	Basaltic
Effect of bubbles	Costa	Costa	Costa	Quane - Russel	Costa	None
Effect of crystals	Costa	Costa	Lejeune - Richet	Dingwell	Melnik - Sparks v2	Costa
Crystallization model	Default	Default	Default	Default	Default	Default
Initial fraction of crystals [vol.%]	NaN	NaN	NaN	NaN	NaN	NaN
Maximum fraction of crystals [vol.%]	0.65	0.65	0.65	0.65	0.65	0.65
Equations of state	Ideal gas	Ideal gas	Ideal gas	Van der Waals	Ideal gas	Ideal gas
Magma fragmentation	Yes	Yes	Yes	Yes	Yes	Yes
α_{cr}	0.7	0.7	0.7	0.7	0.7	0.7
Lateral degassing	No	No	No	No	No	No
Isothermal	Yes	No	Yes	Yes	Yes	Yes
Inlet temperature [°C]	850	900	900	900	1000	1100
Temperature variability [°C]	NaN	NaN	NaN	NaN	NaN	NaN
Inlet overpressure [MPa]	+10.0	+10.0	+10.0	+10.0	+10.0	+10.0
Pressure variability [MPa]	NaN	NaN	NaN	NaN	NaN	NaN
Water content [wt.%]	4.5	4.0	4.0	4.0	4.0	3.0
Water variability [wt.%]	NaN	NaN	NaN	NaN	NaN	NaN
Conduit geometry	Cylinder	DD1	DD2	Cylinder	Cylinder	Dyke
Conduit length [m]	5000	5000	7000	5000	5000	5000
Fixed radius [m]	30	NaN	NaN	15	8	NaN
Radius variability [m]	NaN	NaN	NaN	NaN	NaN	NaN
Major semi-axis [m]	NaN	NaN	NaN	NaN	NaN	200
Minor semi-axis [m]	NaN	NaN	NaN	NaN	NaN	1
Minimum radius [m]	NaN	12	12	NaN	NaN	NaN
Maximum radius [m]	NaN	14	14	NaN	NaN	NaN
Transition depth [m]	NaN	NaN	2000	NaN	NaN	NaN
Length of transition [m]	NaN	NaN	NaN	NaN	NaN	NaN
Mass discharge rate [kg/s]	NaN	NaN	NaN	NaN	NaN	NaN
$\log_{10}(\tau^{(c)})$	+2.0	+2.0	+2.0	+2.0	+2.0	+4.0
$\log_{10}(\tau^{(d)})$	−4.0	−4.0	−4.0	−4.0	−4.0	−4.0
$\log_{10}(\tau^{(p)})$	−4.0	−4.0	−4.0	−4.0	−4.0	−4.0
Outgassing model	Forchheimer	Forchheimer	Forchheimer	Forchheimer	Darcy	Darcy
r_a [m]	0.001	0.001	0.001	0.001	0.001	0.001
$\log_{10}(N_{bd})$	15.0	15.0	13.0	13.0	10.0	10.0

Table 8: Test simulations.

Parameter	S7	S8	S9	S10	S11	S12
Simulation type (modality)	2	2	2	3	3	3
Number of simulations	NaN	NaN	NaN	10	10	10
Composition	Rhyolitic	Trachytic	Andesitic	Dacitic	Phonolitic	Basaltic
Effect of bubbles	Costa	Costa	Costa	Costa	Costa	None
Effect of crystals	Costa	Costa	Melnik - Sparks v1	Vona v1	Melnik - Sparks v2	Costa
Crystallization model	Default	Default	None	Default	Default	Default
Initial fraction of crystals [vol.%]	NaN	NaN	0.2	NaN	NaN	NaN
Maximum fraction of crystals [vol.%]	0.65	0.65	NaN	0.65	0.65	0.65
Equations of state	Ideal gas	Ideal gas	Ideal gas	Ideal gas	Ideal gas	Ideal gas
Magma fragmentation	Yes	Yes	Yes	Yes	Yes	Yes
α_{cr}	0.7	0.7	0.7	0.7	0.7	0.7
Lateral degassing	No	No	No	No	No	No
Isothermal	Yes	Yes	Yes	Yes	Yes	Yes
Inlet temperature [°C]	850	900	1000	900	900	1100
Temperature variability [°C]	NaN	NaN	NaN	10	0	20
Inlet overpressure [MPa]	+10.0	+10.0	+10.0	+10.0	0.0	+10.0
Pressure variability [MPa]	NaN	NaN	NaN	5.0	5.0	5.0
Water content [wt.%]	4.5	4.0	4.5	4.0	4.5	3.0
Water variability [wt.%]	NaN	NaN	NaN	0.5	0.5	0.5
Conduit geometry ([1])	Cylinder	Cylinder	Cylinder	Cylinder	Cylinder	Cylinder
Conduit length [m]	5000	5000	5000	5000	5000	5000
Fixed radius [m] ([2])	30	12	8	12	15	8
Radius variability [m]	NaN	NaN	NaN	1	1	2
Major semi-axis [m]	NaN	NaN	NaN	NaN	NaN	NaN
Minor semi-axis [m]	NaN	NaN	NaN	NaN	NaN	NaN
Minimum radius [m]	NaN	NaN	NaN	NaN	NaN	NaN
Maximum radius [m]	NaN	NaN	NaN	NaN	NaN	NaN
Transition depth [m]	NaN	NaN	NaN	NaN	NaN	NaN
Length of transition [m]	NaN	NaN	NaN	NaN	NaN	NaN
Mass discharge rate [kg/s]	$8 \cdot 10^7$	$2 \cdot 10^7$	$3 \cdot 10^7$	NaN	NaN	NaN
$\log_{10}(\tau^{(c)})$	+2.0	+2.0	+2.0	+2.0	+2.0	+2.0
$\log_{10}(\tau^{(d)})$	−4.0	−4.0	−4.0	−4.0	−4.0	−4.0
$\log_{10}(\tau^{(p)})$	−4.0	−4.0	−4.0	−4.0	−4.0	−4.0
Outgassing model	Forchheimer	Forchheimer	Darcy	Forchheimer	Forchheimer	Darcy
r_a [m]	0.001	0.001	0.001	0.001	0.001	0.001
$\log_{10}(N_{bd})$	15.0	13.0	10.0	15.0	13.0	10.0

([1]) For modalities 2 and 3, Cylinder is the only available conduit geometry.
([2]) For modality 2, it is employed as the initial guess for conduit dimensions.